PHYSICAL REVIEW A **88**, 043427 (2013)

Guiding Rydberg atoms above surface-based transmission lines

P. Lancuba and S. D. Hogan

Department of Physics and Astronomy, University College London, Gower Street, London WC1E 6BT, United Kingdom

(Received 24 September 2013; published 25 October 2013; corrected 1 November 2013)

Beams of helium atoms in selected Rydberg-Stark states with principal quantum number $n = 52$ and electric dipole moments as large as 9910 D have been guided and deflected in the electrostatic fields surrounding surface-based electrical transmission lines. The guided atoms were detected by pulsed-electric-field ionization. Information on their position at the time of ionization was obtained from the flight time of the resulting ions to a microchannel plate detector. Comparison of the experimentally recorded data with the results of numerical calculations of particle trajectories through the guide highlight the sensitivity of the guided signal to the interaction of the atoms with each other and the surrounding 300 K blackbody radiation field.

DOI: 10.1103/PhysRevA.88.043427 PACS number(s): 37.10.Gh, 32.80.Ee, 32.60.+i

I. INTRODUCTION

Atoms and molecules in Rydberg states of high principal quantum number, n, can possess very large electric dipole moments. The maximal electric dipole moment associated with each value n is $|\vec{\mu}_{\max}| \simeq (3/2)n^2 ea_0$, where e is the electron charge and a_0 is the Bohr radius, and approaches 10 000 D for $n = 52$. As was initially suggested by Wing [1] and Breeden and Metcalf [2], and later demonstrated experimentally by Softley and co-workers [3,4], forces can be exerted to efficiently control the translational motion of samples in Rydberg states with these large electric dipole moments using inhomogeneous electric fields. This has led to the realization of Rydberg atom and molecule optics elements including decelerators [5,6], mirrors [7], lenses [8], and traps [9–12], which contribute to the methods, including, e.g., multistage Stark deceleration [13], multistage Zeeman deceleration [14,15], optical Stark deceleration [16], and velocity selection [17], now available for the preparation of cold, velocity-controlled, gas-phase samples of molecules initially traveling in beams.

The techniques for manipulating the translational motion of atoms and molecules in Rydberg states using inhomogeneous electric fields have recently been extended, with development of surface-electrode Rydberg-Stark decelerators and traps [18], to the manipulation of samples close to surfaces. This work, combined with studies of the coherent coupling of gas-phase atoms in Rydberg states to microwave fields in the vicinity of solid-state coplanar transmissions lines [19,20] has opened up a range of exciting prospects for investigations of the interactions of Rydberg atoms and molecules with surfaces [21–23] and for studies of hybrid cavity quantum electrodynamics at vacuum–solid-state interfaces [24].

In a further extension of this surface-based architecture for manipulating the translational motion and the internal quantum states of Rydberg atoms and molecules, we describe here methods for guiding these gas-phase samples in the electrostatic fields surrounding surface-based electrical transmission lines. These transmission-line guides have been exploited to guide and deflect fast beams of helium atoms in Rydberg states with $n = 52$. As their design is based upon those of coplanar electrical transmission lines, they are ideally suited to transporting samples in Rydberg states above microwave circuits and for localizing these samples at precisely defined positions above these circuits. Since the electrode structures of the guides are fabricated on printed circuit boards, the devices described can be readily extended to more elaborate and complex geometries.

II. EXPERIMENT

A schematic diagram of the apparatus used in the experiments described here is presented in Fig. 1. A pulsed supersonic beam of helium (He) atoms in the long-lived, metastable $2\,^3S_1$ state is generated in a dc electric discharge at the exit of a pulsed valve [25]. The discharge takes place between a high-voltage anode, located directly in front of the valve and operated at a potential of +240 V, and the grounded base plate of the valve. The discharge is seeded with electrons emitted from a heated tungsten filament located downstream from the anode. The resulting metastable He beam has a mean longitudinal speed of 1940 m/s.

After passing through a skimmer, the beam enters a pair of metallic electrodes, labeled E1 and E2 in Fig. 1, between which atoms are photoexcited from the $2\,^3S_1$ state to Rydberg states with $n = 52$, in a resonant two-photon excitation scheme via the $3p$ state. This excitation is carried out using focused, copropagating cw laser beams operating at wavelengths close to 389 nm ($\tilde{\upsilon}_{\rm uv} = 25\,709$ cm^{-1} with a power $P_{\rm uv} = 6$ mW) and 788 nm ($\tilde{\upsilon}_{\rm ir} = 12\,690$ cm^{-1} with a power $P_{\rm ir} = 500$ mW). In this photoexcitation region, a homogeneous dc electric field of 0.6 V/cm is generated by applying an electric potential of +0.8 V to E1 while E2 is maintained at a potential of 0 V. The magnitude of this electric field is chosen to permit selective excitation of the individual Stark sublevels at $n = 52$. The relative orientations of the linear polarization of each laser beam and the local electric field vector at the excitation position are chosen to selectively prepare Rydberg states with azimuthal quantum number $|m| = 1$. In this situation the $\ell = 0$ components are absent from the manifold of the Rydberg Stark states (ℓ is the orbital angular momentum quantum number of the Rydberg electron). The resulting Stark map, presented in Fig. 2, was calculated by determining the eigenvalues of the Stark Hamiltonian in a spherical basis including states from $n = 49$ to $n = 55$ [26]. In this calculation, the nonhydrogenic character of the He^+ ion core was accounted for through the inclusion of nonzero quantum defects, δ_ℓ, for the low-angular-momentum Rydberg states. At $n = 52$,

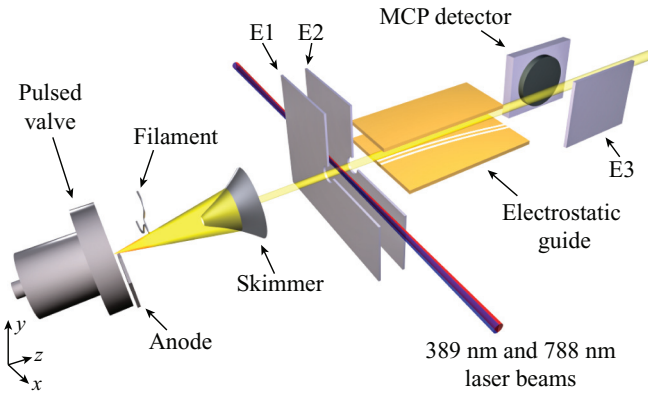

FIG. 1. (Color online) Schematic diagram of the experimental setup (not to scale). Note that part of the plane metal plate positioned above the electrical transmission line in the y dimension to form the electrostatic guide has been removed for clarity.

the relevant quantum defects for the triplet Rydberg states of He are $\delta_p = 0.068\,352$, $\delta_d = 0.002\,888$, $\delta_f = 0.000\,438$, $\delta_g = 0.000\,125$, and $\delta_h = 0.000\,047$ [27].

Following photoexcitation, the beams of helium Rydberg atoms travel through a 3-mm-diameter hole in the center of E2 and toward the part of the apparatus containing the surface-based electrostatic guide. A schematic diagram of a surface-based, coplanar electrical transmission line upon which the geometries of the electrostatic guides are based is displayed in Fig. 3(a). By positioning a parallel plane metal electrode above the surface of the transmission line [Fig. 3(b)], an electric field

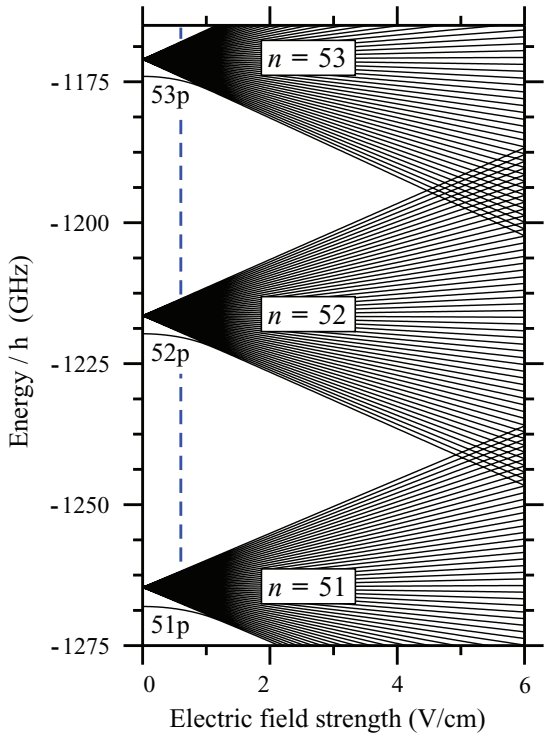

FIG. 2. (Color online) Stark map of the $|m| = 1$ triplet Rydberg states of He for values of n in the range 51–53. The vertical dashed blue line indicates the field of 0.6 V/cm in which photoexcitation was performed in the experiments described.

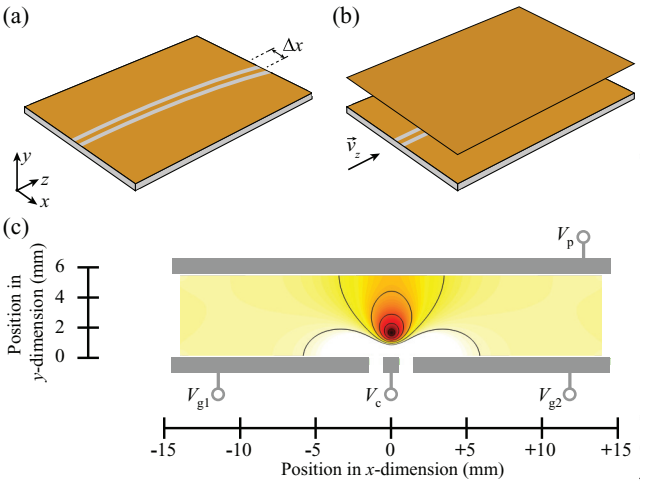

FIG. 3. (Color online) (a) Curved surface-based electrical transmission line. (b) Geometry in which a metallic plate is placed above the surface of the transmission line to permit the generation of an electric field distribution appropriate for guiding samples in Rydberg states. (c) Electric field distribution in the xy plane in the region between the transmission line and metallic plate depicted in (b). The electric field distribution corresponds to that generated when $V_p = V_c = -10$ V and $V_{g1} = V_{g2} = 0$ V. Contours of equal electric field strength are displayed in increments of 5 V/cm starting at 5 V/cm.

minimum can be generated above the center conductor of the transmission line. This is achieved by applying equal, nonzero, electric potentials to the center conductor, V_c, and this plane electrode, V_p, while the outer ground planes of the transmission line, V_{g1} and V_{g2}, are set to 0 V. The electric field distribution, in the xy plane, surrounding a surface-based transmission line with a center conductor of width 1 mm, which is separated from the outer ground planes on either side by a distance of 1 mm, and a parallel plane electrode at a distance of 5.6 mm above the surface of the transmission line in the y dimension, is depicted in Fig. 3(c). In the calculation of this electric field distribution $V_p = V_c = -10$ V and $V_{g1} = V_{g2} = 0$ V. In this figure, contours of equal electric field strength are displayed in increments of 5 V/cm beginning at 5 V/cm. The design of this transmission-line guide, although not identical, has some similarities to electrostatic guides developed by Xia *et al.* [28], for velocity selection of beams of polar molecules, in which a conducting wire is positioned between a pair of parallel-plate electrodes.

The electric field distribution displayed in Fig. 3(c) is designed to efficiently guide atoms in Rydberg-Stark states that are shifted to higher energy with increasing electric field strength, i.e., atoms in "low-field-seeking states." As they travel along the electrostatic guide, atoms in these states continually experience forces directed toward the electric field minimum located 1.7 mm above the surface of the transmission line in the y dimension. Under conditions corresponding to those in Fig. 3(c) the guide has a depth in the xz plane of $E/e \simeq 0.37$ meV (or $E/k_B \simeq 4$ K, where k_B is the Boltzmann constant) for the outermost $n = 52$ Rydberg-Stark states of He. It is worth noting that an equivalent electric field distribution can be generated by applying the nonzero electric potentials of

equal strength to the ground planes while the center conductor and the parallel plane electrode are set to 0 V. In addition, the location of the electric field minimum can be adjusted with respect to the position of the center conductor of the transmission line in the x and y dimensions by generating potential differences $|V_{g1} - V_{g2}| > 0$ and $|V_c - V_p| > 0$, respectively.

In the experiments described here two types of curved transmission lines were used to generate electric field distributions which guide and deflect Rydberg atoms in low-field-seeking states away from their initial axis of propagation and into the positive x dimension. In each case, the structures of the guides were 90-mm-long in the z dimension. The curvature of each transmission line was described by a unique quadratic function in the xz plane with a vertex at the end of each guide closest to the photoexcitation region, and a displacement Δx from the propagation axis of the unguided atomic beam at the end of the guide [see Fig. 3(a)].

After passing through the electrostatic guide the He Rydberg atoms enter the part of the apparatus in front of the microchannel plate detector (MCP), where they are ionized by a pulsed electric field generated by applying a potential of +800 V to the metal electrode labeled E3 in Fig. 1. The resulting He^+ ions are then accelerated in the negative x direction toward the MCP detector. In this configuration, information on the position of the Rydberg atoms in the x dimension at the time of pulsed field ionization (PFI) can be obtained from the time of flight of the He^+ ions to the MCP detector. Atoms located close to the MCP detector at the time of PFI will give rise to an ion signal, which arrives soon after the ionizing electric field is switched on, while the ion signal corresponding to atoms located further from the MCP will arrive later in time.

III. RESULTS

The operation of two transmission-line guides—one with displacement $\Delta x = 2.5$ mm and the other with $\Delta x = 5.0$ mm—was studied by observing changes in the time of flight of the He^+ ions to the MCP detector when equal electric potentials, $V_c = V_p$, of increasing magnitude were applied to the center conductor of the transmission line and the parallel plane electrode. The He^+ time-of-flight signal recorded following photoexcitation to an $n = 52$ Rydberg-Stark state, with a dipole moment of 7930 D, with the $\Delta x = 2.5$ mm guide switched off, i.e., $V_c = V_p = 0$ V, is displayed in Fig. 4(a). The dipole moment of this Rydberg-Stark state corresponds to that of a hydrogenic Stark state at $n = 52$ for which $k = 40$, where $k = n_1 - n_2$, with n_1 and n_2 the parabolic quantum numbers, and $|\mu_{elec}| = (3/2)\,nk\,ea_0$ [29]. The flight time associated with the peak of the signal displayed in Fig. 4(a) is denoted τ_1 (dotted black vertical line) and arrives 585 ns after the application of the ionization pulse.

As the electric potential $V_c = V_p$ is adjusted from −8 to −32 V the Rydberg atoms are guided and deflected away from their initial axis of propagation and into the positive x dimension. The He^+ ions associated with the guided atoms therefore arrive later at the MCP detector, as can be seen in Figs. 4(b)–4(e). For this $\Delta x = 2.5$ mm guide, the increase in the flight time associated with the peak of the He^+ ion signal when the guide was on is $\tau_2 - \tau_1 = 30$ ns. Inserting the

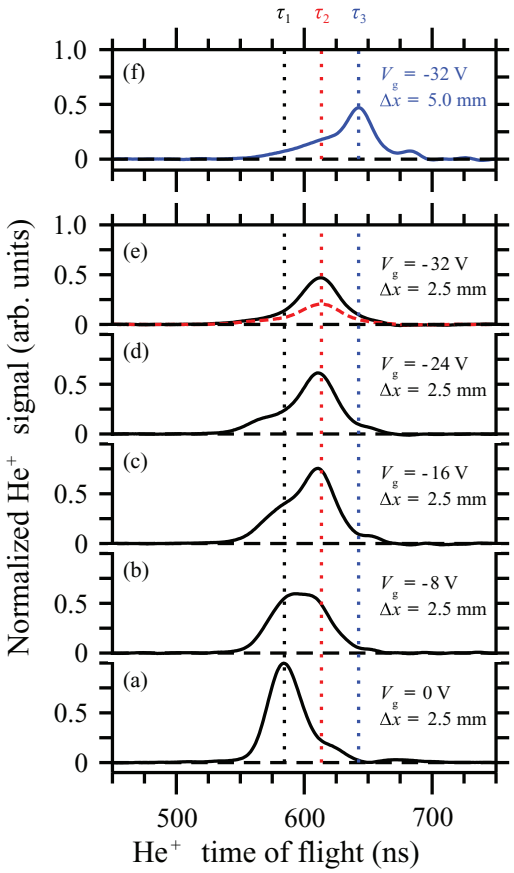

FIG. 4. (Color online) Time-of-flight distribution of He^+ ions detected after PFI of He Rydberg atoms initially excited to states with electric dipole moments of 7930 D that were guided using curved transmission-line guides with displacements $\Delta x = 2.5$ mm (a–e) and $\Delta x = 5.0$ mm (f). The origin of the horizontal axis represents the time at which the ionization pulse was applied. The dotted vertical lines indicate the times at which the maxima of the ion signals corresponding to the unguided atoms (τ_1 black) and those guided using the $\Delta x = 2.5$ mm (τ_2 red) and $\Delta x = 5.0$ mm (τ_3 blue) transmission-line guides were detected. The red dashed time-of-flight distribution in (e) was recorded with $V_g = V_p = +32$ V.

second guide for which $\Delta x = 5.0$ mm in the same apparatus under the same experimental conditions results in a further delay in the arrival time of the He^+ ion signal, as can be seen in Fig. 4(f). By increasing Δx by a factor of 2 for this measurement, the time of flight associated with the peak of the He^+ ion signal (dotted red vertical line) for this second guide is also increased by a factor of two from that in Fig. 4(e), i.e., $\tau_3 - \tau_1 = 2\,(\tau_2 - \tau_1) = 60$ ns. The increase in the signal in the wings of this time-of-flight distribution, with respect to that displayed in Fig. 4(e), indicates a reduction in the acceptance of the guide for the particular states prepared in the experiments and possible losses arising from the adiabatic traversal of avoided crossings in the Stark map.

For each of the measurements presented in Fig. 4, negative electric potentials were applied to the electrodes of the guide. This ensured that the excited Rydberg atoms did not pass through regions of zero electric field strength as they traveled from their position of photoexcitation to the guide. The effect of passing through a zero-field region can, however, be seen

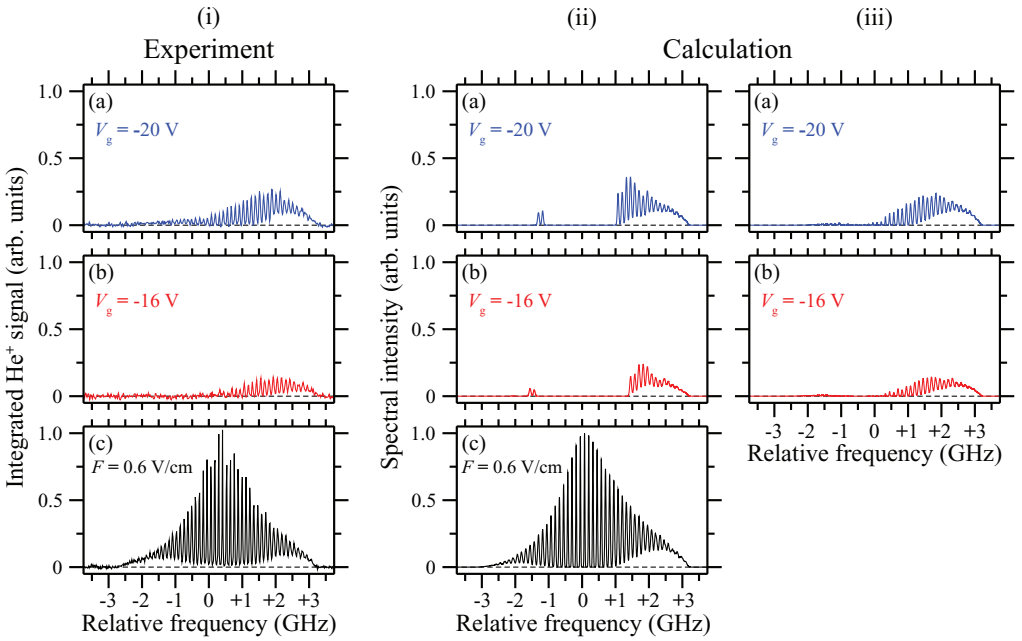

FIG. 5. (Color online) (i) Experimentally recorded, and (ii), (iii) calculated spectra of the $n = 52$, $|m| = 1$ triplet Rydberg-Stark states of He. In each case (c) is a photoexcitation spectrum in the presence of an electric field of 0.6 V/cm, while (b) and (a) are spectra indicating the states in which atoms are efficiently guided when $V_c = V_p = -16$ V and $V_c = V_p = -20$ V, respectively. The calculated spectra in (ii-b) and (ii-a) do not account for effects of state changing arising from the interaction of the atoms with the surrounding blackbody radiation field and collisions between the Rydberg atoms in the guide, while those in (iii-b) and (iii-a) incorporate a simple Monte Carlo model that accounts for these effects.

in Fig. 4(e), where the dashed, red time-of-flight distribution displayed was recorded with $V_c = V_p = +32$ V. Under these conditions the atoms pass through a region of zero electric field strength as they travel through electrode E2 on their trajectories toward the guide. The absence of a quantization axis in this zero-field region leads to scrambling of the Stark states and a resulting loss of population from the initially prepared low-field-seeking states. The change in the intensity of the guided He^+ ion signal by approximately a factor of 0.5 when $V_c = V_p = +32$ V, compared to the case when $V_c = V_p = -32$ V, highlights the importance of maintaining a nonzero electric field quantization axis throughout these experiments.

More detailed information on the dipole acceptance of the transmission-line guides can be obtained by studying the magnitude of the signal associated with the guided atoms as the frequency of the infrared laser is scanned over the $n = 52$ Rydberg-Stark manifold. The results of such measurements, performed using the $\Delta x = 5.0$ mm guide, can be seen in Fig. 5. For reference a photoexcitation spectrum of the $|m| = 1$, hydrogenic Stark states of He, recorded in an electric field of 0.6 V/cm with $V_c = V_p = 0$ V is displayed in Fig. 5(i-c). To record spectra in which only the states with appropriate electric dipole moments for efficient guiding can be identified only the signal associated with guided atoms was detected. This was achieved by setting a time window within the He^+ time-of-flight distribution, between the time τ_3 and $\tau_3 + 30$ ns [see Fig. 4(f)], within which the ion signal was integrated. The resulting integrated signal was then recorded as the frequency of the infrared laser was scanned. To further improve the separation between the signals from the guided and unguided atoms, two circular metallic slits with diameters of 3 mm were placed after the guide before the PFI region. One of these slits was centered on the axis of propagation of the unguided atomic beam while the other, displaced from this axis in the x dimension, was centered on the end of the $\Delta x = 5.0$ mm guide. The narrow integration window, combined with the spatial separation provided by the circular slits permitted only guided atoms to be detected, as can be seen by comparing the signal intensity within the time range in Figs. 4(a) and 4(f). The photoexcitation spectrum recorded under these conditions with $V_c = V_p = -16$ V is displayed in Fig. 5(i-b). As expected, only atoms in outer low-field-seeking states, with the largest electric dipole moments, on the high-energy side of the $n = 52$ Stark manifold are present in this spectrum. When the electric potential applied to the guide was increased to $V_c = V_p = -20$ V the electric field gradients of the guide also increased and states closer to the center of the Stark manifold, with smaller electric dipole moments, were also guided, as can be seen in Fig. 5(i-a).

The operation of the guide can be further characterized by comparison of the experimental spectra in Fig. 5(i) with calculated spectra that include the results of numerical simulations of the trajectories of Rydberg atoms through the guide. The results of these calculations are presented in Figs. 5(ii) and 5(iii). In each of these calculated spectra, the spectral intensities of the Rydberg-Stark states at photoexcitation [see Fig. 5(ii-c)] were determined from the $\ell = 2$ components of the eigenvectors associated with each state in the appropriate energy range in Fig. 2 [26].

At the edges of the experimentally recorded spectrum presented in Fig. 5(i-c) the spectral features associated with

transitions to the outer Stark states with the largest electric dipole moments are broadened, giving rise to a nonzero spectral intensity between individual features in these spectral regions. This is an effect of inhomogeneities in the photoexcitation volume and can be crudely accounted for by including an electric field gradient of ~ 0.05 V/cm^2 across the ensemble of excited atoms in the calculations [see Fig. 5(ii-c)]. By convoluting this calculated spectrum with the guiding efficiency for each Rydberg-Stark state, the spectra presented in Figs. 5(ii-b) and 5(ii-a) were calculated for $V_c = V_p = -16$ V and $V_c = V_p = -20$ V, respectively.

The calculated spectra presented in Fig. 5(ii) exhibit the same general appearance as those recorded experimentally; i.e., the atoms are seen to be most efficiently guided when initially photoexcited to the outermost low-field-seeking Stark states with the largest electric dipole moments. However, there are two notable features of the calculated spectra which differ from the experimental observations. These are (1) a sharp cutoff in the spectral intensity of the low-field-seeking states on the high-energy side of the Stark manifold for dipoles below 4860 and 3750 D in Figs. 5(ii-b) and 5(ii-a), respectively, and (2) the presence in each spectrum of two intensity maxima corresponding to transitions to high-field-seeking states. As they travel through the guide, atoms in low-field-seeking Stark states follow trajectories on the outside of the guide where the radial electric field gradient is positive. Since this guiding field gradient approaches zero with increasing distance from the electric field minimum, beams of atoms with a narrow longitudinal velocity distributions will only be efficiently guided if their dipole moments are larger than a particular threshold value. In states with dipole moments below this threshold value, which is dependent upon the electric potentials V_c and V_p, the Rydberg atoms will escape from the guide leading to a cutoff in the acceptance. This effect can be seen in the experimental data and the results of the calculations. However, the sharp cutoff seen in the calculated spectra is not apparent in the experimental data. In addition, the high-field-seeking states that follow quasistable trajectories around the inside of the guide, where the radial electric field gradient is negative, and are present in the calculated spectra are also absent in the experimental data.

In the experimental measurements presented in Fig. 5(i) the flight time of the Rydberg atoms from the photoexcitation region to the position where they were detected by PFI was 85 μs. During this time the atoms interact with each other and undergo transitions driven by the room-temperature blackbody radiation field with which they interact. As has been discussed in the literature previously with regard to experiments involving electrostatically trapped Rydberg atoms and molecules [11], in the presence of an external electric field blackbody transitions between Rydberg-Stark states occur primarily between states with different values of n, but with similar electric dipole moments. As a result these blackbody transitions between Rydberg states do not lead to a significant loss of atoms from the guide, but instead to a modification of the Stark-state acceptance.

In the experiments described here the metal plates of the surface-based transmission line and parallel plane electrode form a parallel-plate microwave cavity. This cavity strongly modifies the electromagnetic mode structure in the vicinity of the guide and consequently has a significant effect on the blackbody radiation spectrum with which the Rydberg atoms interact as they travel through the guide. This, combined with the strong dependence of the blackbody transition rates on the magnitude of the electric field experienced by the atoms, makes it difficult to construct a complete numerical model to account for the effects of blackbody transitions on the spectra of the guided Rydberg atoms. However, by implementing a simple hydrogenic Monte Carlo model in which the value of k, which determines the electric dipole moment $|\mu_{elec}| = (3/2)\, nk\, ea_0$, changes by ± 1 at a predefined rate, the effects of state changing, arising from blackbody transitions and collisions between the guided atoms, on the calculated spectra displayed in Fig. 5(ii) can be elucidated. The results of incorporating this simple model, with a $|\Delta k| = 1$ transition rate of $\sim 10^7$ s^{-1}, into the calculation of the spectra of the guided atoms are presented in Figs. 5(iii-b) and 5(iii-a) for $V_c = V_p = -16$ V and $V_c = V_p = -20$ V, respectively. From these calculated spectra it can be seen that the comparatively small changes in electric dipole moment that result from state changing give rise to a broadening of the dipole acceptance of the guide. The sharp cutoff in acceptance which is apparent in Figs. 5(ii-b) and 5(ii-a) is no longer observed and the calculated spectra are closer in appearance to those recorded experimentally. In addition, the narrow range of high-field-seeking states which undergo quasistable trajectories through the guide appear not to be sufficiently stable to be efficiently guided if the magnitude of their dipole moments changes during their trajectory through the guide.

It is important to note that the k-changing rate included in the calculation of the spectra in Fig. 5(iii) does not represent the mean 300 K blackbody depopulation rate of the Rydberg-Stark states in the experiments. It does not distinguish between state changing that arises from collisions between the Rydberg atoms in the guide and blackbody transitions and does not explicitly account for transitions for which $|\Delta k| > 1$ or transitions between states of the same electric dipole moment but different values of n. To disentangle these processes and to minimize the effects of blackbody radiation in future experiments (1) the central part of the experimental apparatus can be cooled to reduce the blackbody photon occupation numbers at the microwave frequencies to which the Rydberg states are most sensitive and (2) the electromagnetic mode structure of the space surrounding the guide can be engineered to modify these blackbody photon occupation numbers from their values in free space [30]. For electrostatically trapped samples of hydrogen Rydberg atoms, it has been shown experimentally that at blackbody temperature close to 10 K, the purity of Rydberg-Stark states with values of n around 30 is maintained for several hundred microseconds [31]. However, by appropriately engineering the electromagnetic mode structure of the environment in which the atoms are located similar conditions may be achievable at higher temperatures.

IV. CONCLUSIONS

In conclusion, fast beams of helium atoms in high Rydberg states have been efficiently guided and deflected in

the inhomogeneous electrostatic fields surrounding electrical transmission lines. The effects of nonadiabatic transitions when the excited Rydberg atoms traverse regions of zero electric field strength have been identified and highlight the importance of maintaining an electric field quantization axis throughout the entire trajectory of the Rydberg atoms in these experiments. By comparing experimentally recorded photoexcitation spectra corresponding to the signal from the guided atoms, with calculations that account for the particle trajectories through the guide and a simple model to treat the effects of blackbody radiation, the important role that collisions and blackbody radiation play when these experiments are performed in a room-temperature environment has been demonstrated. The simple geometries of these transmission-line guides makes them very scalable, and the possibility of integrating them into chip-based microwave circuits is expected to show them playing an important role in the future in surface-based architectures for manipulating Rydberg atoms and molecules.

ACKNOWLEDGMENTS

We thank Rafid Jawad and Alan Suganuma for their assistance in preparing the electrical transmission lines and developing the detection electronics, respectively. This work was supported financially by the Department of Physics and Astronomy and the Faculty of Mathematical and Physical Sciences at UCL.

[1] W. H. Wing, Phys. Rev. Lett. **45**, 631 (1980).
[2] T. Breeden and H. Metcalf, Phys. Rev. Lett. **47**, 1726 (1981).
[3] D. Townsend, A. L. Goodgame, S. R. Procter, S. R. Mackenzie, and T. P. Softley, J. Phys. B: At. Mol. Opt. Phys. **34**, 439 (2001).
[4] S. R. Procter, Y. Yamakita, F. Merkt, and T. P. Softley, Chem. Phys. Lett. **374**, 667 (2003).
[5] E. Vliegen, H. J. Wörner, T. P. Softley, and F. Merkt, Phys. Rev. Lett. **92**, 033005 (2004).
[6] E. Vliegen and F. Merkt, J. Phys. B: At. Mol. Opt. Phys. **38**, 1623 (2005).
[7] E. Vliegen and F. Merkt, Phys. Rev. Lett. **97**, 033002 (2006).
[8] E. Vliegen, P. Limacher, and F. Merkt, Eur. Phys. J. D **40**, 73 (2006).
[9] S. D. Hogan and F. Merkt, Phys. Rev. Lett. **100**, 043001 (2008).
[10] S. D. Hogan, Ch. Seiler, and F. Merkt, Phys. Rev. Lett. **103**, 123001 (2009).
[11] Ch. Seiler, S. D. Hogan, H. Schmutz, J. A. Agner, and F. Merkt, Phys. Rev. Lett. **106**, 073003 (2011).
[12] S. D. Hogan, Ch. Seiler, and F. Merkt, J. Phys. B: At. Mol. Opt. Phys. **46**, 045303 (2013).
[13] H. L. Bethlem, G. Berden, and G. Meijer, Phys. Rev. Lett. **83**, 1558 (1999).
[14] N. Vanhaecke, U. Meier, M. Andrist, B. H. Meier, and F. Merkt, Phys. Rev. A **75**, 031402(R) (2007).
[15] E. Narevicius, A. Libson, C. G. Parthey, I. Chavez, J. Narevicius, U. Even, and M. G. Raizen, Phys. Rev. Lett. **100**, 093003 (2008).
[16] R. Fulton, A. I. Bishop, and P. F. Barker, Phys. Rev. Lett. **93**, 243004 (2004).
[17] S. A. Rangwala, T. Junglen, T. Rieger, P. W. H. Pinkse, and G. Rempe, Phys. Rev. A **67**, 043406 (2003).
[18] S. D. Hogan, P. Allmendinger, H. Saß mannshausen, H. Schmutz, and F. Merkt, Phys. Rev. Lett. **108**, 063008 (2012).
[19] S. D. Hogan, J. A. Agner, F. Merkt, T. Thiele, S. Filipp, and A. Wallraff, Phys. Rev. Lett. **108**, 063004 (2012).
[20] J. D. Carter and J. D. D. Martin, arXiv:1308.1945 [Phys. Rev. A (to be published)].
[21] V. Sandoghdar, C. I. Sukenik, E. A. Hinds, and S. Haroche, Phys. Rev. Lett. **68**, 3432 (1992).
[22] S. B. Hill, C. B. Haich, Z. Zhou, P. Nordlander, and F. B. Dunning, Phys. Rev. Lett. **85**, 5444 (2000).
[23] G. R. Lloyd, S. R. Procter, and T. P. Softley, Phys. Rev. Lett. **95**, 133202 (2005).
[24] M. Wallquist, K. Hammerer, P. Rabl, M. Lukin, and P. Zoller, Phys. Scr. **T137**, 014001 (2009).
[25] T. Halfmann, J. Koensgen, and K. Bergmann, Meas. Sci. Technol. **11**, 1510 (2000).
[26] M. L. Zimmerman, M. G. Littman, M. M. Kash, and D. Kleppner, Phys. Rev. A **20**, 2251 (1979).
[27] W. C. Martin, Phys. Rev. A **36**, 3575 (1987).
[28] Y. Xia, Y. Yin, H. Chen, L. Deng, and J. Yin, Phys. Rev. Lett. **100**, 043003 (2008).
[29] T. F. Gallagher, *Rydberg Atoms* (Cambridge University Press, Cambridge, U.K., 1994).
[30] A. G. Vaidyanathan, W. P. Spencer, and D. Kleppner, Phys. Rev. Lett. **47**, 1592 (1981).
[31] Ch. Seiler, S. D. Hogan, and F. Merkt, Chimia **66**, 208 (2012).